International Journal of Thermal Sciences 191 (2023) 108352

Contents lists available at ScienceDirect

International Journal of Thermal Sciences

journal homepage: www.elsevier.com/locate/ijts

Direct numerical simulation of the fully developed turbulent free convection flow in an asymmetrically heated vertical channel

Jordi Pallares [a,*], Alexandre Fabregat [a], Chengwang Lei [b]

[a] Departament d'Enginyeria Mecànica, Universitat Rovira i Virgili, Av. Països Catalans 16, 43007, Tarragona, Spain
[b] Centre for Wind, Waves and Water, School of Civil Engineering, The University of Sydney, Sydney, NSW, 2006, Australia

ARTICLE INFO

Keywords:
Turbulent flow
Natural convection
Vertical channel
Asymmetrical heating
Direct numerical simulation

ABSTRACT

We report direct numerical simulations of the fully developed turbulent natural convection flow of a Boussinesq fluid ($Pr = 0.71$) in a vertical channel. One wall is heated with a constant heat flux and the other is assumed to be perfectly insulated. Simulations were performed at three different Rayleigh numbers ($Ra = 5 \times 10^5$, 10^6 and 5×10^6). Predictions of the time averaged velocities, temperatures and intensities of the fluctuations agree with experiments reported in the literature. Under the fully developed flow conditions considered in this study the shear stress is greater on thermally active wall than that on the adiabatic wall, but the turbulent intensities and the turbulent shear stress are greater near the insulated wall. Conversely, the intensities of the temperature fluctuations and turbulent heat fluxes are higher near the thermally active wall than those near the adiabatic wall. Contrary to the vertical channel with constant but different wall temperatures, where buoyancy and turbulent shear dominate the generation of turbulent kinetic energy, in the asymmetrically heated channel the turbulent shear stress is the principal mechanism of turbulent kinetic energy production as in a forced convection channel flow.

1. Introduction

Turbulent free convection in vertical channels has implications in a large number of engineering situations, including air cooling of electronic equipment [1], transformers, power supplies or components mounted on vertically arranged circuit boards [2], cooling of nuclear reactor fuel elements [3] and photovoltaic cells [4] or the passive heating and ventilation of buildings using Trombe walls [5] and solar chimneys [6,7].

A vertical differentially heated plane channel with two infinite isothermal walls at different temperatures achieves statistically steady and fully developed state with anti-symmetric velocity and temperature profiles. It is a configuration that has received considerable interest to analyze the characteristics of turbulent vertical natural convection flows because of its simplicity [8–13]. In numerical simulations periodic boundary conditions can be applied directly in the streamwise and spanwise directions of the domain to simulate fully developed flow conditions. The turbulent statistics, flow structures and proper scalings for the mean and turbulent flow variables have been reported for this flow configuration up to $Ra = 10^9$ and the effect of the Prandtl number (for $1 \leq Pr \leq 100$) has been recently analyzed in Ref. [14].

The effect of asymmetrical heating of a vertical channel also has been analyzed because of its application in many passive cooling systems with a vertical heated surface cooled by the buoyancy-driven flow in an open-ended channel. The developing laminar flow in this configuration was numerically and experimentally analyzed in Ref. [15] and experimentally in Ref. [16], and an analytical solution for the laminar fully developed flow conditions was given in Ref. [17]. In this case the flow exhibits an asymmetrical velocity profile with the velocity maximum displaced close to the wall with the larger heat flux. The effect of the interplate spacing on the laminar water flow between one wall held at a constant temperature and an adiabatic wall was analyzed in Ref. [18] using experiments and numerical simulations. The turbulent flow for this set of thermal boundary conditions was considered in Ref. [19]. These authors compared numerical simulations, based on the Reynolds Averaged Navier-Stokes (RANS) equations, with their experiments in a developing air flow in a 3 m high and 1 m wide channel with a 0.1 m separation between the vertical walls. Thermal stratification and radiation heat transfer effects on the laminar flow with a wall heated at a constant heat flux were numerically simulated in Ref. [20], and important variations of the flow characteristics and extension of flow reversal were observed near the exit of the channel.

* Corresponding author.
E-mail address: jordi.pallares@urv.cat (J. Pallares).

https://doi.org/10.1016/j.ijthermalsci.2023.108352
Received 28 December 2022; Received in revised form 15 March 2023; Accepted 11 April 2023
Available online 15 April 2023

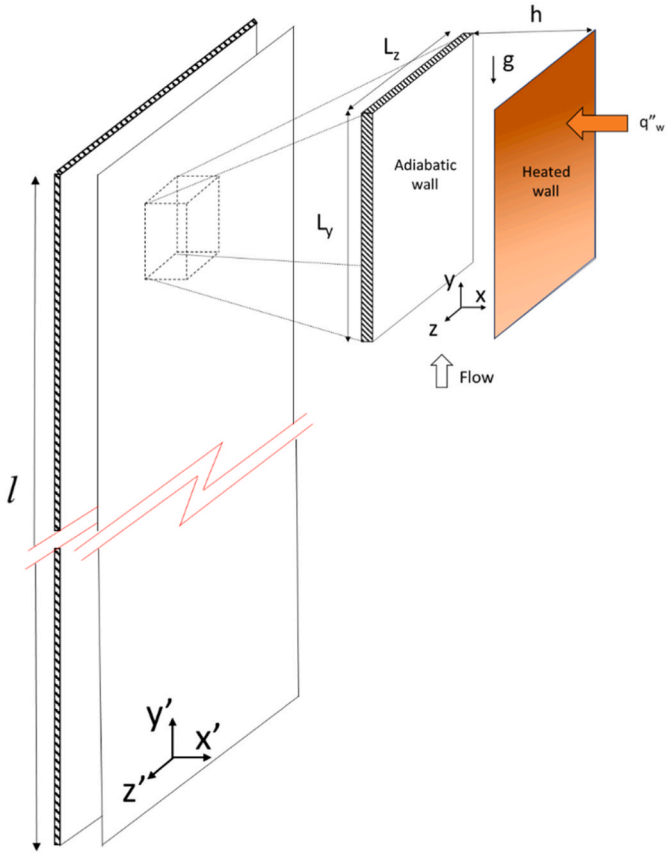

Fig. 1. Physical model and schematic of the computational domain.

The measurements of the turbulent air flow in a vertical channel ($l =$ 5-m high and 1-m wide) with one wall heated with a constant heat flux were reported in Refs. [21,22]. The separation of the walls (h) was varied between 40 and 200 mm and these authors reported detailed measurements of the developing velocity and temperature profiles, turbulence quantities and averaged heat transfer and mean flow rates over a wide range of Rayleigh numbers based on the constant wall heat flux and the separation of the walls ($10^3 < Ra\ (h/l) < 10^8$). Simulations of the flow using a RANS model [23] were found in agreement with the measurements [21] by tuning the turbulence intensity at the inlet of the channel. Large-Eddy Simulations of the experiments [21] were reported in Ref. [24] where the numerical predictions of the developing flow are compared with the measurements in terms of mean velocity and temperature profiles and Nusselt numbers. The flow reversals observed near the bottom inlet and the top outlet of the channel have been also examined and analyzed in Refs. [25,26].

To our knowledge the turbulent flow in an asymmetrically heated vertical channel has not been investigated using Direct Numerical Simulations (DNS). In this study we report DNS of the turbulent flow at relatively low Rayleigh numbers with an identical configuration of wall boundary conditions as those in the experiments [21,22] and the RANS simulations [23].

2. Physical and mathematical models

The channel under consideration has two large parallel vertical walls separated by a distance h. One wall is heated uniformly with a constant heat flux (q''_w) and the other is perfectly insulated (see Fig. 1). We consider a Newtonian fluid ($Pr = 0.71$) with constant physical properties. The variation of the density with temperature is assumed to be linear following the Boussinesq approximation. For air at ambient temperature and pressure ($Pr = 0.71$) the validity of this approximation is limited to temperature differences up to about 30 °C [27]. Radiation heat transfer and viscous dissipation are neglected. We assume that the channel has a vertical dimension (l), large enough to reach fully developed hydrodynamic and thermal flow conditions. The vertical (streamwise) coordinate y' has its origin at the bottom of the channel where the temperature is uniform and constant, T_0. The x' coordinate is in the wall-normal direction, and the z' coordinate is in the spanwise direction.

For uniform and constant heat flux on the thermally active wall and under the steady state approximation, the linear evolution of the fluid bulk temperature (T_b) along the vertical axial (y') direction is given by the following equation

$$\frac{dT_b}{dy'} = \frac{q''_w}{C_p \rho_0 V_b h} = \frac{T_b(y' = l) - T_0}{l} \tag{1}$$

where ρ_0 is the reference density, C_p is the heat capacity and V_b and T_b are, respectively, the bulk velocity and the bulk temperature. Equation (1) assumes that the bulk velocity is constant. These averaged quantities are defined as

$$V_b = \frac{1}{A}\int_A v\, dA \tag{2}$$

$$T_b = \frac{1}{A V_b}\int_A T v\, dA \tag{3}$$

where A is the cross-stream area (i.e., the flow area in the $x' - z'$ plane). At a distance sufficiently far from the channel inlet, we define a periodic computational domain of dimensions $h \times L_y \times L_z$ at $z' = 0$, as shown in Fig. 1, to consider the statistically fully developed flow and the thermal field. The system of coordinates attached to the computational domain is constituted by the x (normal to the wall), y (axial or streamwise) and z (spanwise) directions (see Fig. 1). To apply the periodic boundary conditions along the axial direction the vertical force per unit volume defined as

$$f = -\frac{\partial p}{\partial y} - \rho g \tag{4}$$

needs to be periodic. Pressure is divided into a periodic part $\tilde{p}$ and a function, $r(y)$, that depends exclusively on y.

$$p(x, y, z, t) = \tilde{p}(x, y, z, t) + r(y) \tag{5}$$

Similarly, temperature is divided into a periodic part ($\tilde{T} - \tilde{T}_{b,i}$) and the linear evolution of the average temperature along y.

$$T(x, y, z, t) = \left(\tilde{T}(x, y, z, t) - \tilde{T}_{b,i}\right) + \frac{q''_w}{C_p \rho_0 V_b h}\, y + T_0 \tag{6}$$

where $\tilde{T}_{b,i}$ is the bulk value of $\tilde{T}$ at the inlet of the computational domain located at $y = 0$ (see Fig. 1). Using the linear dependence of density on temperature, with β, the thermal expansion coefficient

$$\rho = \rho_0[1 - \beta(T - T_0)] \tag{7}$$

and using Eqs. (4), (5) and (7), the force per unit volume is

$$f = -\frac{\partial \tilde{p}}{\partial y} - \frac{dr(y)}{dy} + \rho_0 g\left[1 - \beta\left(\tilde{T} - \tilde{T}_{b,i}\right) - \beta\frac{dT_b}{dy}y\right] \tag{8}$$

Defining the periodic force per unit volume as

$$\tilde{f} = -\frac{\partial \tilde{p}}{\partial y} + \rho_0 g \beta \tilde{T} \tag{9}$$

Equation (8) can be rewritten as

$$f = \tilde{f} - \frac{dr(y)}{dy} + \rho_0 g \beta \frac{dT_b}{dy} y - \rho_0 g \beta \tilde{T}_{b,i} \tag{10}$$

Imposing periodicity on f and integrating the right-hand side of Eq.

(10), $r(y)$ can be obtained as

$$r(y) = \rho_0 g\beta \frac{dT_b}{dy}\frac{y^2}{2} - \rho_0 g\beta \widetilde{T}_{b,i} y - \rho_0 g y + C \tag{11}$$

Imposing the hydrostatic pressures at the inlet and outlet of the channel to be $r(y' = 0) = p_0$ and $r(y' = l) = p_0 - \rho_0 g l$, respectively, the externally imposed pressure head can be used to determine $r(y)$ and $\widetilde{T}_{b,i}$.

$$r(y) = \rho_0 g\beta \frac{dT_b}{dy}\frac{y^2}{2} - \rho_0 g\beta \widetilde{T}_{b,i} y - \rho_0 g y + p_0 \tag{12}$$

$$\widetilde{T}_{b,i} = \frac{dT_b}{dy}\frac{l}{2} = \frac{q''_w\, l}{2\, C_p \rho_0 V_b h} \tag{13}$$

The governing equations have been non-dimensionalized with the separation of the walls (h) and ($\alpha\sqrt{Ra}/h$) as length and velocity scales, respectively. That is,

$$x_i^* = \frac{x_i}{h}, u_i^* = \frac{u_i}{(\alpha/h)\sqrt{Ra}}, p^* = \frac{p}{\rho_0(\alpha/h)^2 Ra} \tag{14}$$

The non-dimensional temperature is

$$\theta^* = \frac{\widetilde{T}}{q''_w\, h/k} \tag{15}$$

and the non-dimensional bulk temperature at the inlet of the computational domain, obtained from Eq. (13), is

$$\theta^*_{b,i} = \frac{l/h}{2V_b^*\sqrt{Ra}} \tag{16}$$

Note that the non-dimensional bulk temperature depends on the ratio of the length of the channel (l) and the separation of the walls (h). This ratio has been set to 100, which corresponds to channels with a length of several meters and with a separation of the walls of several centimeters.

Applying these normalisations to the dimensional governing equations, we obtain the following non-dimensional equations as

$$\frac{\partial u_i^*}{\partial x_i^*} = 0 \tag{17}$$

$$\frac{\partial u_i^*}{\partial t^*} + \frac{\partial u_j^* u_i^*}{\partial x_j^*} = -\frac{\partial p^*}{\partial x_i^*} + \frac{Pr}{\sqrt{Ra}}\frac{\partial^2 u_i^*}{\partial x_j^* \partial x_j^*} + Pr\,\theta^* \tag{18}$$

and

$$\frac{\partial \theta^*}{\partial t^*} + \frac{\partial u_i^* \theta^*}{\partial x_i^*} = -\frac{u_i^*}{V_b^*\sqrt{Ra}}\delta_{i2} + \frac{1}{\sqrt{Ra}}\frac{\partial^2 \theta^*}{\partial x_i^* \partial x_i^*} \tag{19}$$

where $Ra = g\beta(q''_w h/k)h^3/\nu\alpha$ and $Pr = \nu/\alpha$ are the Rayleigh and Prandtl numbers, respectively, and δ_{i2} is the Kronecker's delta. The decomposition of the temperature field into a periodic part and the averaged linear variation along the vertical direction (see Eq. (6)) generates the first term on the right of the non-dimensional thermal energy balance (Eq. (19)). To satisfy the macroscopic thermal energy within the computational domain, at each time step we numerically computed the non-dimensional bulk temperature at the inlet of the computational domain as:

$$\theta^*_{b,i,c} = \frac{1}{Lz\, V_b^*}\int_0^1 \int_{-Lz/2}^{Lz/2} \theta^*(x^*, i, z^*, t^*) v^*(x^*, i, z^*, t^*)\, dz^* dx^* \tag{20}$$

To enforce the theoretical value of the bulk temperature at the inlet of the computational domain, $\theta_{b,i}$, given in Eq. (16), the entire thermal field was corrected, to satisfy the value of the bulk temperature at the inlet of the computational domain using the computed value $\theta_{b,i,c}$, that is,

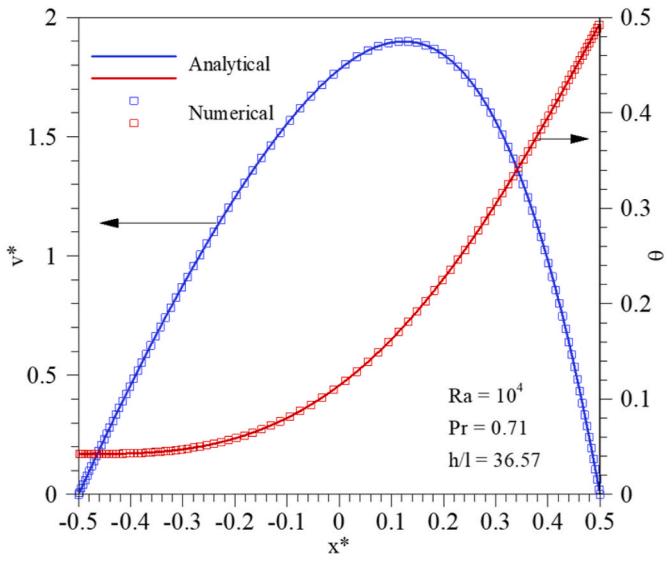

Fig. 2. Non-dimensional velocity and temperature profiles for a laminar flow.

$$\theta^*_{corrected}(x^*, y^*, z^*, t^*) = \theta^*(x^*, y^*, z^*, t^*) - \left(\theta^*_{b,i,c} - \theta^*_{b,i}\right) \tag{21}$$

Non-slip boundary conditions are imposed on the walls. On the adiabatic wall, the zero gradient of temperature is assumed ($\partial\theta^*/\partial x^* = 0$) and on the thermally active wall a constant gradient is set ($\partial\theta^*/\partial x^* = -1$). Periodic boundary conditions for u_i^*, p^* and θ^* are used on the remaining boundaries of the computational domain.

The solver 3DINAMICS has been used to solve the governing equations (Eq. 17 to 19) with their respective boundary conditions. Diffusive and convective terms are both spatially discretized using a second-order central differencing scheme and temporally integrated using second-order Crank-Nicolson and Adams-Bashforth schemes respectively. The pressure and velocity fields are decoupled by solving the Poisson equation using an efficient multigrid solver. The code has been adopted successfully for direct numerical simulations of turbulent forced [28] and natural [10,29] convection flows in channels.

The mesh adopted in the simulations has 100 × 141 × 121 grid nodes distributed in a computational box with dimensions h x12.5 h x6.28 h along the wall-normal, streamwise and spanwise directions, respectively. Uniform mesh spacings are used along the streamwise ($\Delta y^* = 0.089$) and spanwise ($\Delta z^* = 0.053$) directions and the grid is stretched near the walls ($0.0017 \leq \Delta x^* \leq 0.023$). These grid spacings give similar resolutions in terms of the Kolmogorov scale (η) as other direct numerical simulations reported in the literature for the differentially heated vertical channel [13]. For example at $Ra = 5 \times 10^5$, $\Delta_{x,y,z} < 4.3\eta$ near the center of the channel and $\Delta_x < 6.0\eta$ and $\Delta_{z,y} < 3.6\eta$ near the adiabatic wall. To check the influence of the grid resolution on the results, a simulation at the highest Rayleigh number $Ra = 5 \times 10^6$ has been conducted with a coarser grid (91 × 121 × 100). It is found that the differences in predicted bulk quantities and wall shear stresses compared to those obtained with the finer grid (100 × 141 × 121) are smaller than 3%. The time-step for the simulations is set to $\Delta t^* = 0.01$ and turbulent statistics are computed once the flow is statistically fully developed over approximately 210 nondimensional time units. This time duration corresponds to about 25 throughflows along the streamwise length of the channel ($L_y = 12.5h$).

To confirm that the code and the boundary conditions were correctly implemented we simulated the steady laminar flow ($Ra = 10^4$, $Pr = 0.71$ and $l/h = 36.57$) using the above computational domain and grid resolution. Fig. 2 shows the numerically predicted velocity and temperature profiles and the corresponding analytical solutions given in Ref. [17] along the wall-normal direction (x). The velocity profile is

Table 1
Parameters of the simulations.

Ra	V_b^*	θ_b^*	θ_{aw}^*	θ_{hw}^*	$Re_{\tau(aw)}$	$Re_{\tau(hw)}$	$Re = h\,V_b/\nu$
5×10^5	1.53	0.0456	0.0105	0.225	57.2	74.1	1520
10^6	1.42	0.0349	0.00804	0.193	73.0	90.5	1995
5×10^6	1.17	0.0190	0.00523	0.130	128	143	3680

asymmetric with respect to the channel centre and exhibits a maximum displaced towards the heated wall. Note that the agreement between the simulated (symbols) and the theoretical profiles (lines) is excellent.

3. Results and discussion

3.1. Mean velocities, temperature and fluctuation intensities

Table 1 summarizes the relevant dimensionless numbers for the three simulations of the turbulent flow at three different Rayleigh numbers carried out in this study. The values of the spatial and time averaged temperatures at the adiabatic wall (θ_{aw}^*) and at the heated wall (θ_{hw}^*), the Reynolds numbers based on the local friction velocity ($Re_{\tau(aw)} = hu_{\tau(aw)}/2\nu$ and $Re_{\tau(hw)} = hu_{\tau(hw)}/2\nu$), and the Reynolds number (Re) based on the bulk velocity are also given in Table 1. Fig. 3 shows the time averaged velocity and temperature profiles. The measurements reported in Ref. [21] ($h = 50$ mm, $q_w'' = 208$ W/m^2, $y' = 3865$ mm and $l/h = 100$, $Ra \sim 4.5 \times 10^6$) and [22] ($h = 50$ mm, $q_w'' = 202$ W/m^2, $y' = 3840$ mm and $l/h = 100$, $Ra \sim 4.6 \times 10^6$) at the highest Rayleigh number ($Ra = 5 \times 10^6$) are also plotted for comparison. The asymmetry of the velocity profile increases, as the Rayleigh number is increased, and the maximum velocity is progressively displaced towards the heated wall. According to the data shown in Table 1, the wall shear stresses on both walls increase at a similar rate ($Re_{\tau(aw)} \sim Ra^{0.35}$ and $Re_{\tau(hw)} \sim Ra^{0.29}$) with the Rayleigh number. The non-dimensional temperatures (Fig. 3b) at both walls decrease as the Rayleigh number is increased according to the adopted temperature scaling $\theta^* = \frac{\widetilde{T}}{q_w'' h/k} = \frac{\widetilde{Tg\beta h^3}}{Ra\ \nu\alpha}$. The temperature of the adiabatic wall, located at $x^* = -0.5$, progressively decreases reaching a temperature similar to the inlet temperature ($\theta^* \sim \theta_{b,i}^*$) and the non-dimensional temperature at the heated wall, located at $x^* = 0.5$, also decreases as the Rayleigh number is increased at a higher rate ($\theta_{hw}^* \sim Ra^{-0.24}$).

The velocity profiles are shown in wall coordinates in Fig. 4. Note that according to the adopted coordinate system (refer to Fig. 1) $x^+ = (0.5 - |x^*|)hu_\tau/\nu$ is the wall-normal direction in wall coordinates. The profiles corresponding to the adiabatic and heated walls are plotted in Fig. 4a and b, respectively. The Reynolds numbers based on the local friction velocities indicated in Table 1 have been used for the scalings.

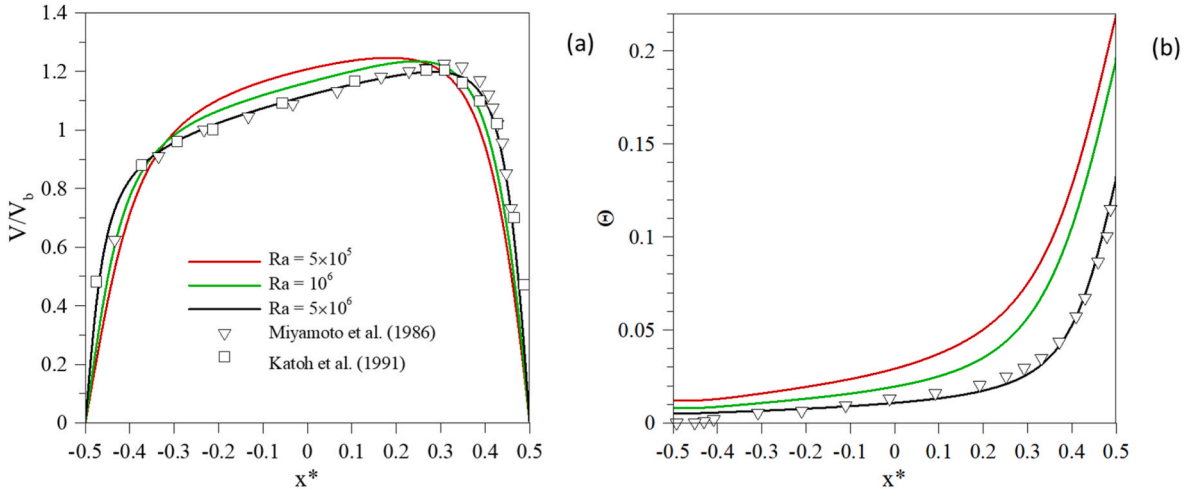

Fig. 3. Time averaged (a) velocity and (b) temperature profiles.

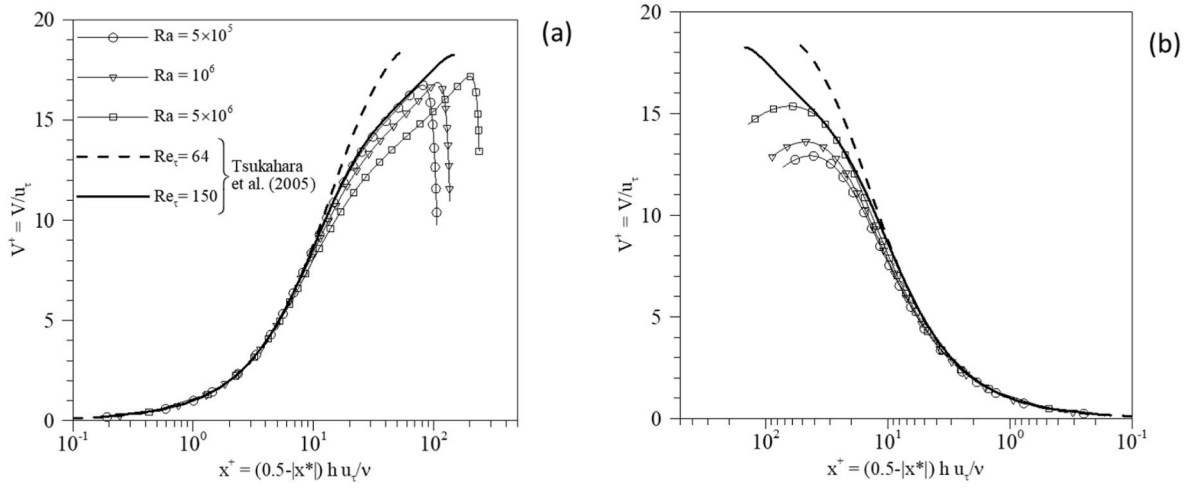

Fig. 4. Time averaged velocity profiles in wall coordinates (a) near the adiabatic wall and (b) near the heated wall.

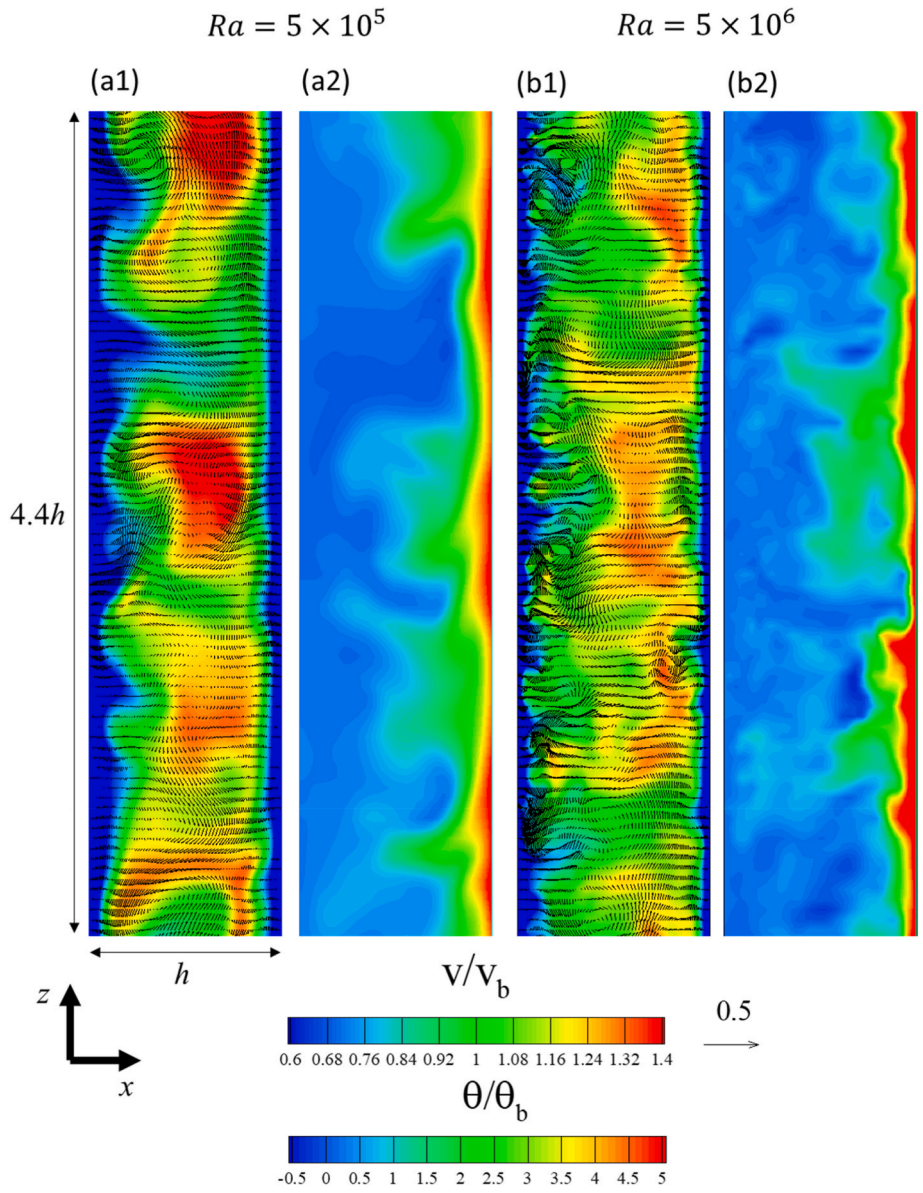

Fig. 5. Instantaneous velocity (a1 and b1) and thermal (a2 and b2) fields scaled with the corresponding bulk quantities indicated in Table 1 at $Ra = 5\times 10^5$ (a1 and a2) and $Ra = 5 \times 10^6$ (b1 and b2). Note that the spanwise dimension of the plots is smaller than the spanwise dimension of the computational domain ($L_z = 6.28h$).

For comparison purposes the profiles from DNS of a pressure-driven isothermal turbulent channel flow at low Reynolds number [30] have been included in the plots. In general, the profiles at the three Rayleigh numbers considered exhibit a viscous sublayer for $x^+ < 5$. The profiles near the adiabatic wall show a logarithmic region with a slope of 2.5 corresponding to a von Kármán constant of $\kappa = 0.4$ in agreement with the relatively low Reynolds number (see Table 1). The extent of this region close to the adiabatic wall increases as the Rayleigh number is increased while the profiles near the heated wall do not exhibit a fully logarithmic region.

To illustrate the transient flow structures Fig. 5 shows examples of the instantaneous velocity and temperature fields in a cross stream plane at the minimum and maximum Rayleigh numbers respectively. Fig. 5a1 and 5b1 show the vectors of the cross stream velocity components (u and w) superimposed onto the contours of the streamwise velocity component (v). The contours of the instantaneous temperature, at the same time instant, are plotted in Fig. 5a2 and 5b2. To make the plots at the two different Rayleigh numbers more comparable, velocities and temperatures have been scaled with the corresponding bulk values, indicated in Table 1. Fig. 5 shows spots of high streamwise velocity closer to the heated wall than to the adiabatic wall distributed along the spanwise (z) direction. Note that at the highest Rayleigh number (Fig. 5 b1) these spots are closer to the heated wall than those at the lowest Rayleigh number (Fig. 5 a1) in agreement with the time-averaged velocity profiles shown in Fig. 3a. These high streamwise momentum spots are positively correlated with relatively large values of instantaneous temperature. The comparison of the contours and the cross stream vector fields of Fig. 5a ($Ra = 5 \times 10^5$) and 5b ($Ra = 5 \times 10^6$) reveals a distinct increase of fine scale flow structures and of the cross stream velocity intensities, especially near the adiabatic wall, at the highest Rayleigh number compared to the lowest Rayleigh number.

The normal and shear stresses are plotted in Fig. 6a and b, respectively. In general, the turbulence intensities are larger near the adiabatic wall than those near the heated wall, which is in agreement with measurements [22]. As in a differentially heated channel, the axial turbulent Reynolds stress is the largest normal turbulent stress followed by the spanwise and the normal to the wall components (Fig. 6a). The weak and positive turbulent shear stress near the heated wall indicates that

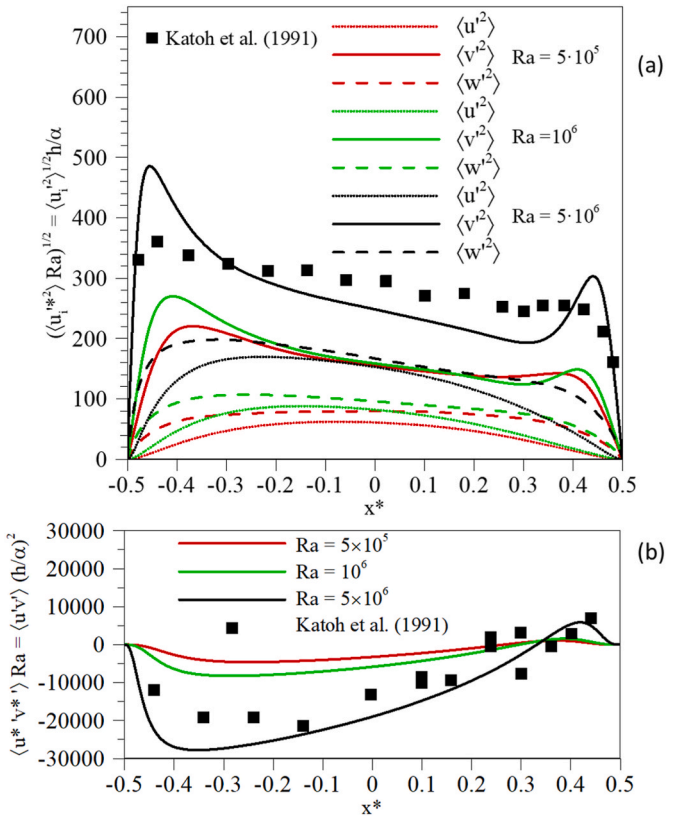

Fig. 6. (a) Normal Reynolds stresses. (b) Turbulent shear stress.

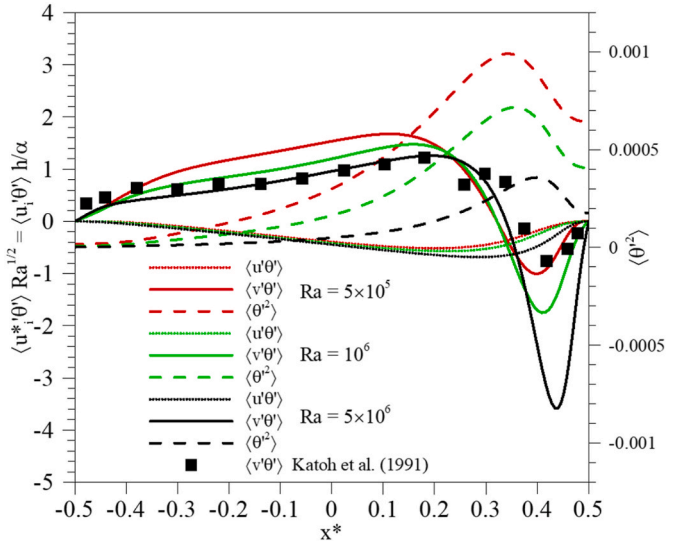

Fig. 7. Turbulent heat fluxes and temperature fluctuations.

positive fluctuations are correlated with wall-normal velocities away from the wall. Both the present numerical simulations and measurements [22] suggest that the streamwise fluctuations (v') are mostly negatively correlated with the wall-normal velocity component (u) across the channel section in agreement with the time averaged velocity profile shown in Fig. 3a. For example, near the adiabatic wall, a (negative) fluctuation of the wall-normal velocity component towards the adiabatic wall implies a (positive) fluctuation of the streamwise velocity component.

The intensities of the fluctuations of temperature and the turbulent heat fluxes are shown in Fig. 7. The intensities of the fluctuations of temperature peak near the heated wall, located at $x^* = 0.5$, and vanish near the insulated wall, located at $x^* = -0.5$. The normal to the wall turbulent heat flux ($u'\theta'$), which is significantly smaller than the streamwise turbulent heat flux, is negative in the whole cross section of the channel according to the monotonic increase of the time averaged temperature with the normal to the wall direction (x) shown in Fig. 3b. In this case a positive fluctuation of the wall-normal velocity component produces a negative fluctuation of the temperature. At the highest Rayleigh number ($Ra = 5 \times 10^6$) the streamwise turbulent heat flux, $v'\theta'$, plotted in Fig. 7, as the turbulent shear stress, plotted in Fig. 6b changes the sign approximately at the position where the maximum of the time averaged velocity occurs (at $x^* \approx 0.32$). This behavior was also observed in measurements [22] although the reported values near the wall were significantly smaller.

3.2. Momentum and turbulence kinetic energy budgets

The time averaged vertical momentum budget for fully developed flow conditions can be written as

$$0 = -\frac{d\overline{u^{*'}v^{*'}}}{dx^*} + \frac{Pr}{\sqrt{Ra}}\frac{d^2V^*}{dx^{*2}} + Pr\,\Theta^* \tag{22}$$

The different terms are the turbulent transport, viscous diffusion and the buoyancy term. Fig. 8a shows the horizontal profiles of these terms at $Ra = 5 \times 10^5$. The relative distribution of the terms at $Ra = 10^6$ and $Ra = 5 \times 10^6$ is the same as that at $Ra = 5 \times 10^5$ and consequently the budgets at these higher Rayleigh numbers have been omitted for brevity. For comparison purposes, the corresponding profiles for the fully developed flow in a differentially heated vertical channel with a cooled isothermal wall at $x^* = -0.5$ and a heated isothermal wall at $x^* = 0.5$ at $Ra = 5.4 \times 10^5$ reported in Ref. [8] are plotted in Fig. 8b. Note that for the differentially heated channel the time averaged flow is ascending for $x^* > 0$ (i.e. positive buoyancy) and descending for $x^* < 0$ (i.e. negative buoyancy). It can be seen that for both flows viscous diffusion opposes buoyancy. For the asymmetric heating (Fig. 8a) buoyancy balances the viscous diffusion near the heated wall ($x^* \approx 0.5$). Near the adiabatic wall ($x^* \approx -0.5$), the turbulent transport balances viscous diffusion as in the case of the isothermal pressure-driven plane turbulent channel flow [31] and this explains the logarithmic region of the time-averaged velocity profiles, shown in Fig. 4a, near this wall. In the central part of the channel ($x^* \approx 0$), the viscous diffusion reaches small values and the turbulent transport is a sink of momentum to balance buoyancy. This is also the case for the differentially heated channel where the turbulent transport is a sink even near the isothermal walls.

The turbulent kinetic energy budget for a vertical fully developed natural convection flow is

$$0 = -\frac{d\overline{u^{*'}p^{*'}}}{dx^*} - \frac{1}{2}\frac{d}{dx^*}\left(\overline{u^{*'3}} + \overline{v^{*'2}u^{*'}} + \overline{w^{*'2}u^{*'}}\right) + \frac{Pr}{\sqrt{Ra}}\frac{d^2K^*}{dx^{*2}} - \overline{u^{*'}v^{*'}}\frac{dV^*}{dx^*} + Pr\overline{\theta^{*'}v^{*'}} - \frac{Pr}{\sqrt{Ra}}\frac{\partial\overline{u_i^{*'}u_i^{*'}}}{\partial x_j^* x_j^*} \tag{23}$$

The different terms of Eq. (23) from left to right are the pressure transport, the turbulent transport by turbulent velocity fluctuations or turbulent convection, the viscous diffusion, the shear production, the buoyancy production and the turbulent kinetic energy dissipation. The horizontal profiles of these terms are plotted in Fig. 9a for $Ra = 5 \times 10^5$. As in Fig. 8, the corresponding profiles for the differentially heated channel at $Ra = 5.4 \times 10^5$ are shown in Fig. 9b [8]. In the flow with asymmetric heating the production of turbulent kinetic energy is dominated by the shear stress production term. Near the walls the turbulent transport terms and the viscous diffusion, together with the shear production term balance the dissipation. The relative contribution of these terms is very similar to that in a fully developed forced convection

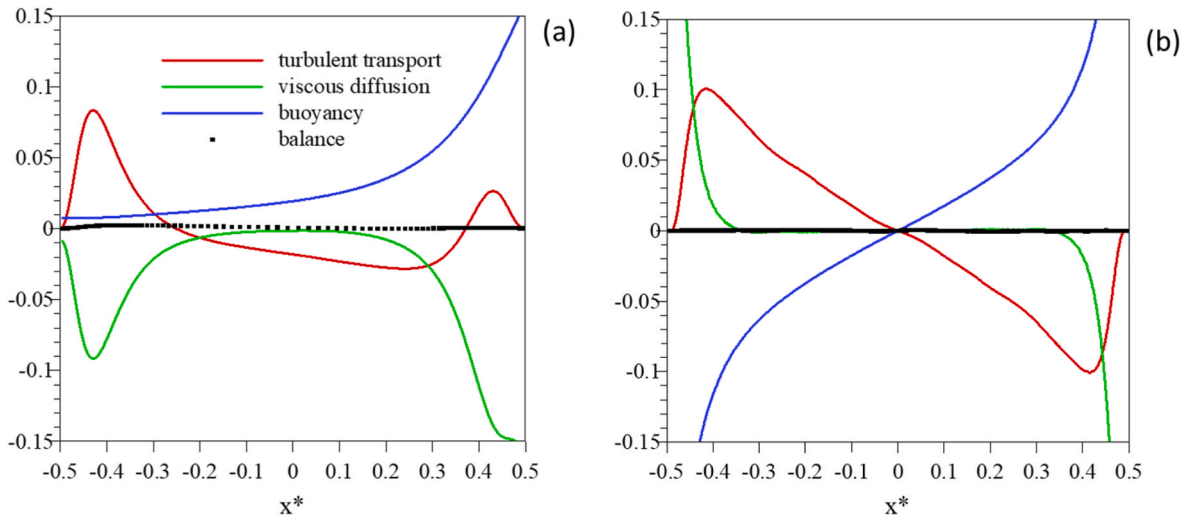

Fig. 8. Time averaged vertical momentum budget. (a) Asymmetrically heated channel at $Ra = 5 \times 10^5$. (b) Differentially heated channel at $Ra = 5.4 \times 10^5$ (Versteegh and Nieuwstadt, 1998).

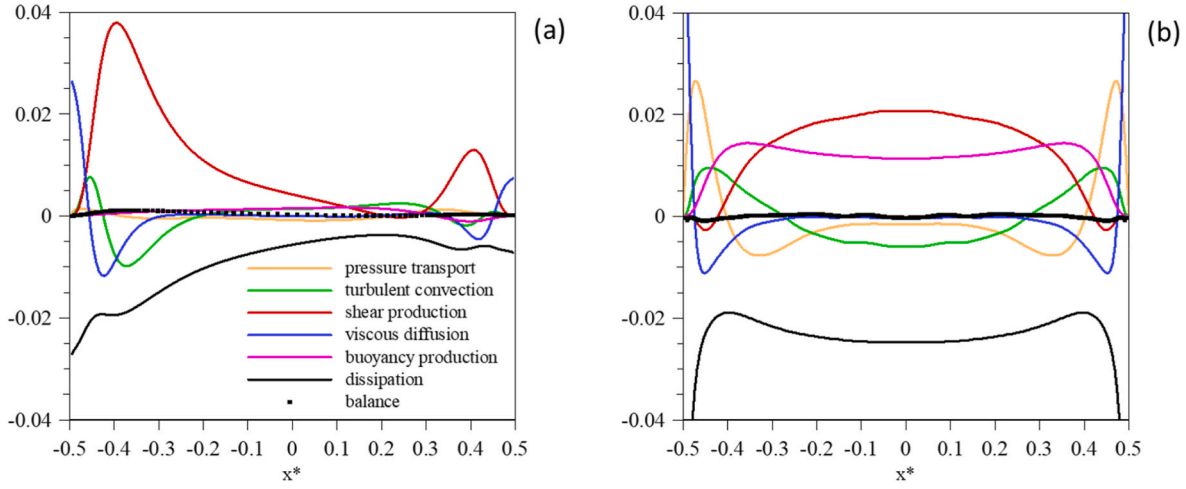

Fig. 9. Turbulent kinetic energy budget. (a) Asymmetrically heated channel at $Ra = 5 \times 10^5$. (b) Differentially heated channel at $Ra = 5.4 \times 10^5$ (Versteegh and Nieuwstadt, 1998).

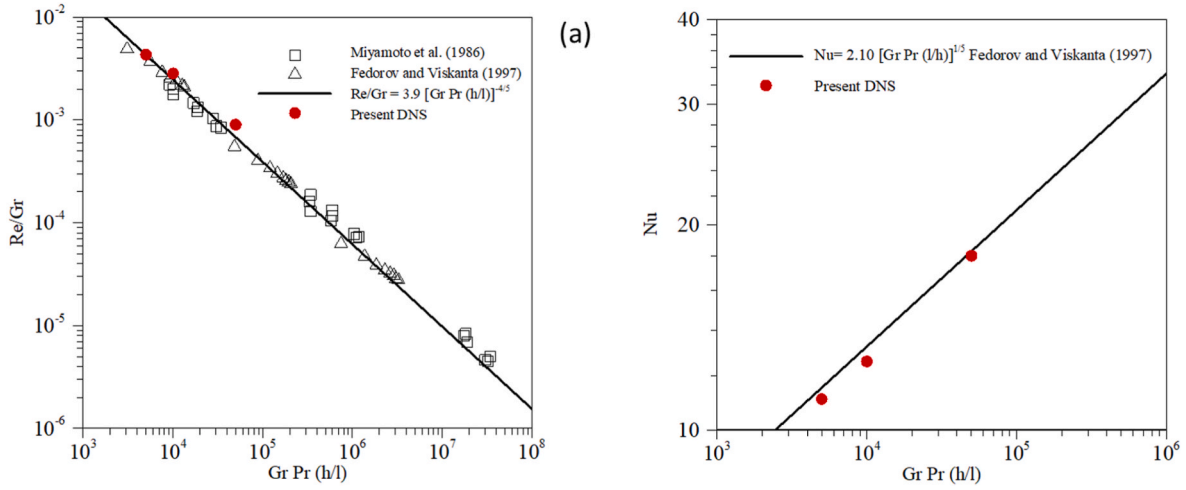

Fig. 10. Nondimensional (a) flow rate and (b) Nusselt number as a function of the modified Rayleigh number ($Ra^* = Gr\,Prh/l$).

plane channel flow [31]. The other terms (i.e. the pressure transport and buoyancy production) have a minor contribution to the budget. The scenario is completely different for the differentially heated channel with important contributions to the production of turbulent kinetic energy from both the buoyancy production and shear production terms in the central part of the channel and from the turbulent transport terms (pressure and turbulent convection) near both heated and cooled walls.

3.3. Mean flow and heat transfer rates

Fig. 10a and b shows, respectively, the non-dimensional flow rate (Re/Gr) and Nusselt number as a function of the modified Rayleigh number ($Ra^* = Gr\,Prh/l$) for the three simulations performed. The non-dimensional flow rate is usually expressed in the literature as the ratio between the Reynolds number ($Re = V_b h/\nu$) and the Grashof number ($Gr = g\beta(q''_w h/k)h^3/\nu^2$). The experimental measurements [21] for $h/l =$ 0.01, 0.02 and 0.04, the numerical results based on the solution of the RANS equations reported in Ref. [23] ($h/l =$ 0.025, 0.05 and 0.1) are also included in Fig. 10a. It can be seen that the present predictions are in excellent agreement with the correlation proposed in Refs. [21,23]. The averaged Nusselt number ($Nu = \frac{h_c}{k}\frac{2h}{} = \frac{2h\,q''_w}{k(T_w - T_b)}$ is plotted in Fig. 10b. Again, the present predictions agree well with the correlation proposed in Ref. [23].

4. Conclusions

Direct numerical simulations of the fully developed buoyancy-driven turbulent air flow ($Pr = 0.71$) in a vertical channel are reported. One of the walls of the channel is heated with a constant heat flux while the other is considered perfectly adiabatic. The fully developed flow conditions have been modelled by applying periodic boundary conditions in a computational box and by adjusting the inlet temperature at the inlet of the computational domain to enforce the theoretical value predicted by macroscopic thermal energy balance. The asymmetric time averaged velocity profile generates larger wall shear stresses on the heated wall than those on the adiabatic wall. Further, temperature fluctuations and turbulent heat fluxes are higher near the heated wall. However, turbulence intensities and turbulent shear stress are larger near the adiabatic wall than those near the heated wall. The larger turbulence intensities and turbulent shear stresses lead to a logarithmic region near the adiabatic wall in the time averaged velocity profiles scaled with the local friction velocity and plotted in wall coordinates. Contrary to the turbulent flow in a differentially heated channel, the turbulent kinetic energy in the asymmetrically heated channel is predominantly produced by shear, which attains, together with the dissipation, large values near the adiabatic wall. The predictions of the flow rate generated by buoyancy and the heat transfer rate on the heated wall are in excellent agreements with those reported in the literature.

Declaration of competing interest

The authors declare that they have no known competing financial interests or personal relationships that could have appeared to influence the work reported in this paper.

Data availability

Data will be made available on request.

Acknowledgments

The financial support of the Spanish Ministerio de Ciencia, Innovación y Universidades, through the grants PID2020-113303 GB-C21 and RTI2018-100907-A-I00 (MCIU/AEI/FEDER), and of the Generalitat de Catalunya, through the grants 2017-SGR-1234 and 2021-SGR-00732, is greatly acknowledged. This study has also been funded by the Australian Research Council through Discovery Project grant DP210102901. JP thanks the support of the Faculty of Engineering, The University of Sydney during his stay in Sydney.

References

[1] R. Bessaih, M. Kadja, Turbulent natural convection cooling of electronic components mounted on a vertical channel, Appl. Therm. Eng. 20 (2) (2000) 141–154.
[2] K.M. Kelkar, D. Choudhury, Numerical prediction of periodically fully developed natural convection in a vertical channel with surface mounted heat generating blocks, Int. J. Heat Mass Tran. 36 (5) (1993) 1133–1145.
[3] D. Ito, Y. Saito, Natural convection cooling characteristics in a plate type fuel assembly of Kyoto University Research Reactor during loss of coolant accident, Ann. Nucl. Energy 90 (2016) 1–8.
[4] C. Daverat, H. Pabiou, C. Menezo, H. Bouia, S. Xin, Experimental investigation of turbulent natural convection in a vertical water channel with symmetric heating: flow and heat transfer, Exp. Therm. Fluid Sci. 44 (2013) 182–193.
[5] D. Wang, L. Hu, H. Du, Y. Liu, J. Huang, Y. Xu, J. Liu, Classification, experimental assessment, modeling methods and evaluation metrics of Trombe walls, Renew. Sustain. Energy Rev. 124 (2020), 109772.
[6] E. Bacharoudis, M.G. Vrachopoulos, M.K. Koukou, D. Margaris, A.E. Filios, S. A. Mavrommatis, Study of the natural convection phenomena inside a wall solar chimney with one wall adiabatic and one wall under a heat flux, Appl. Therm. Eng. 27 (13) (2007) 2266–2275.
[7] R. Khanal, C. Lei, Solar chimney—a passive strategy for natural ventilation, Energy Build. 43 (8) (2011) 1811–1819.
[8] T.A.M. Versteegh, F.T.M. Nieuwstadt, Turbulent budgets of natural convection in an infinite, differentially heated, vertical channel, Int. J. Heat Fluid Flow 19 (2) (1998) 135–149.
[9] T.A.M. Versteegh, F.T.M. Nieuwstadt, A direct numerical simulation of natural convection between two infinite vertical differentially heated walls scaling laws and wall functions, Int. J. Heat Mass Tran. 42 (19) (1999) 3673–3693.
[10] J. Pallares, A. Vernet, J.A. Ferre, F.X. Grau, Turbulent large-scale structures in natural convection vertical channel flow, Int. J. Heat Mass Tran. 53 (19–20) (2010) 4168–4175.
[11] P. Kiš, H. Herwig, The near wall physics and wall functions for turbulent natural convection, Int. J. Heat Mass Tran. 55 (9–10) (2012) 2625–2635.
[12] C.S. Ng, D. Chung, A. Ooi, Turbulent natural convection scaling in a vertical channel, Int. J. Heat Fluid Flow 44 (2013) 554–562.
[13] C.S. Ng, A. Ooi, D. Lohse, D. Chung, Vertical natural convection: application of the unifying theory of thermal convection, J. Fluid Mech. 764 (2015) 349–361.
[14] C.J. Howland, C.S. Ng, R. Verzicco, D. Lohse, Boundary layers in turbulent vertical convection at high Prandtl number, J. Fluid Mech. (2022) 930.
[15] W. Aung, L.S. Fletcher, V. Sernas, Developing laminar free convection between vertical flat plates with asymmetric heating, Int. J. Heat Mass Tran. 15 (11) (1972) 2293–2308.
[16] B.W. Webb, D.P. Hill, High Rayleigh number laminar natural convection in an asymmetrically heated vertical channel, J. Heat Tran. 111 (1989) 649–656.
[17] W. Aung, Fully developed laminar free convection between vertical plates heated asymmetrically, Int. J. Heat Mass Tran. 15 (8) (1972) 1577–1580.
[18] E.M. Sparrow, L.F.A. Azevedo, Vertical-channel natural convection spanning between the fully-developed limit and the single-plate boundary-layer limit, Int. J. Heat Mass Tran. 28 (10) (1985) 1847–1857.
[19] T. Yilmaz, S.M. Fraser, Turbulent natural convection in a vertical parallel-plate channel with asymmetric heating, Int. J. Heat Mass Tran. 50 (13–14) (2007) 2612–2623.
[20] D. Ramalingom, P.H. Cocquet, A. Bastide, Numerical study of natural convection in asymmetrically heated channel considering thermal stratification and surface radiation, Numer. Heat Tran., Part A: Applications 72 (9) (2017) 681–696.
[21] M. Miyamoto, Y. Katoh, J. Kurima, H. Sasaki, Turbulent free convection heat transfer from vertical parallel plates, in: C.L. Tien, V.P. Carey, J.K. Ferrell (Eds.), Heat Transfer 1986, Proceedings of the Eight International Heat Transfer Conference, San Francisco, California, USA, Hemisphere, Whasington, 1986, pp. 1593–1598.
[22] Y. Katoh, M. Miyamoto, J. Kurima, S. Kaneyasu, Turbulent free convection heat transfer from vertical parallel plates: effect of entrance bell-mouth shape, JSME international journal. Series II, Fluids engineering, heat transfer, power, combustion, thermophysical properties 34 (4) (1991) 496–501.
[23] A.G. Fedorov, R. Viskanta, Turbulent natural convection heat transfer in an asymmetrically heated, vertical parallel-plate channel, Int. J. Heat Mass Tran. 40 (16) (1997) 3849–3860.
[24] G.E. Lau, G.H. Yeoh, V. Timchenko, J.A. Reizes, Numerical investigation of passive cooling in open vertical channels, Appl. Therm. Eng. 39 (2012) 121–131.
[25] D. Ospir, C. Popa, C. Chereches, G. Polidori, S. Fohanno, Flow visualization of natural convection in a vertical channel with asymmetric heating, Int. Commun. Heat Mass Tran. 39 (4) (2012) 486–493.
[26] K.M. Kim, D.H. Nguyen, G.H. Shim, D.W. Jerng, H.S. Ahn, Experimental study of turbulent air natural convection in open-ended vertical parallel plates under asymmetric heating conditions, Int. J. Heat Mass Tran. 159 (2020), 120135.
[27] D.D. Gray, A. Giorgini, The validity of the Boussinesq approximation for liquids and gases, Int. J. Heat Mass Tran. 19 (5) (1976) 545–551.

[28] J. Pallares, A. Vernet, F.X. Grau, Effect of the instantaneous turbulent flow structures on the particle distribution near the wall of a channel, Eur. J. Mech. B Fluid 46 (2014) 144–153.
[29] J. Pallares, F.X. Grau, Particle dispersion in a turbulent natural convection channel flow, J. Aerosol Sci. 43 (2012) 45–56.
[30] T. Tsukahara, Y. Seki, H. Kawamura, D. Tochio, DNS of turbulent channel flow at very low Reynolds numbers, in: Proceedings of the Forth International Symposium on Turbulence and Shear Flow Phenomena, Williamsburg, USA, 2005, pp. 935–940.
[31] J. Kim, P. Moin, R. Moser, Turbulence statistics in fully developed channel flow at low Reynolds number, J. Fluid Mech. 177 (1987) 133–166.